Journal of Materials Chemistry A

ROYAL SOCIETY OF CHEMISTRY

PAPER

View Article Online
View Journal | View Issue

Cite this: J. Mater. Chem. A, 2020, 8, 14644

Metal–organic framework-based foams for efficient microplastics removal†

Yong-Jun Chen,[a] Yifa Chen,*[ab] Chang Miao,[a] Yi-Rong Wang,[a] Guang-Kuo Gao,[a] Ru-Xin Yang,[a] Hong-Jing Zhu,[a] Jian-Hui Wang,[a] Shun-Li Li[a] and Ya-Qian Lan *[a]

Received 12th May 2020
Accepted 30th June 2020

DOI: 10.1039/d0ta04891g

rsc.li/materials-a

Microplastics are a worldwide problem that poses a giant threat to organisms in the ecosystem and even to human health. The removal of microplastics is a severe challenge that needs to be solved urgently. Herein, a series of zirconium metal–organic framework-based foam materials with interpenetrated pores, high MOF uniformity and excellent durability have been successfully fabricated and applied in simulated microplastics removal in water or seawater conditions. They can be applied to various types and concentrations of microplastics suspensions. It is worth noting that the best of them, UiO-66-OH@MF-3, can efficiently remove microplastics with an efficiency of up to 95.5 ± 1.2% and can maintain high performance in recycling and large-quantity filtration experiments. Besides, we proposed an automatic filtration system powered by sunlight and accomplished it on the lab-scale. The high performances of these foam materials combined with the new concept of automatic filtration systems might shed some light on the development of novel techniques for microplastics removal.

Introduction

Waste plastics have become a huge environmental crisis worldwide.[1] In 2018, the total consumption of plastics reached ~8 billion tons and only a small amount (~9%) was recycled.[2,3] The discarded plastics can stay in the environment for a long time and some will break down into microplastics through mechanical or biological processes.[4,5] In 2004, for the first time, the concept of "microplastics" was proposed in published journals, referring to plastic fragments less than 5 mm [6] in diameter, also called "$PM_{2.5}$ in the sea". Every year, the total production of plastic is ~275 million tons and ~5 to 13 million tons of them enter the sea, resulting in yearly increases in the amount of microplastics.[7,8] Besides, tremendous human activity-producing wastes like microbeads in cleansers, the abrasion of tires and synthetic textiles from washing machines will aggravate the crisis.[9,10] In 2014, there were ~15 to 51 trillion pieces of microplastics with a total weight of ~9.3×10^4 to 2.36×10^5 tons floating in the sea.[11] In particular, the small-sized microplastics possessing high specific surface area can strongly absorb contaminants (*e.g.*, polychlorinated biphenyls or bisphenol A, *etc.*) and might be ingested by animals like plankton or seabirds and reach into tissues or even the blood cells.[12] Humans are at the top of the food chain and can potentially accumulate microplastics in the body, bringing unpredictable threats to human health.[13]

To treat the microplastics problem, controlling the sources of microplastics is of vital concern to everyone in the world. However, it requires a long period of time and takes generations of effort. In contrast, the development of novel removal techniques might be a more promising strategy for the immediate treatment of the microplastics problem. In current techniques, the common methods applied in the filtration of solid particles from the aqueous phase include typical filtration, microfiltration, ultrafiltration or nanofiltration.[14] For typical filtration techniques (*e.g.*, filter paper), the relatively large pore size (20–25 μm) might only filter out microplastics of dozens of microns, and cannot efficiently treat microplastics of a few microns or nanometers.[15] For microfiltration (0.1–1 μm), ultrafiltration (2–100 nm) or nanofiltration (~2 nm), although they have potential for the filtration of microplastics of micron or nanometer size, they still have some disadvantages as follows: (1) the small pore size might result in slow filtration rates and even pore plugging, which would be difficult in large-scale treatment. (2) The filtration processes are generally conducted under high pressure, which might require high cost and energy consumption. (3) Their regeneration generally requires the use of high-pressure recoil technology, which further increases the difficulty of recovery.[16] Although there are some pioneering techniques like membrane bioreactors,[17] adsorption on green microalgae,[18] electrocoagulation[19] and conventional activated sludge,[20] which possess potential in microplastics removal, the

[a]Jiangsu Collaborative Innovation Centre of Biomedical Functional Materials, Jiangsu Key Laboratory of New Power Batteries, School of Chemistry and Materials Science, Nanjing Normal University, Nanjing 210023, P. R. China. E-mail: chyf927821@163.com; yqlan@njnu.edu.cn

[b]Changzhou Institute of Innovation & Development, Nanjing Normal University, Nanjing 210023, P. R. China

† Electronic supplementary information (ESI) available. See DOI: 10.1039/d0ta04891g

exploration of this field is still in its early stages. Besides, these methods have some inevitable disadvantages like energy demand, disability to treat small-sized microplastics, difficulty in large-scale treatment and lack of reproducibility.[21] Therefore, the exploration of novel strategies for the efficient removal of microplastics is in high demand.

Metal–organic frameworks (MOFs) are porous, crystalline materials constructed by the assembly of metal ions and organic ligands, which have attracted significant research interest in various applications like gas storage, separation, catalysis, sensing and contaminant removal, *etc.*[22–33] Owing to the high porosity, tunable structure and rich functionality, MOFs possessing various metal centers, tunable functional groups and charge are promising in pollutant treatment.[34–36] Therefore, MOFs might provide an alternative for microplastics removal. However, MOFs with a crystalline and fragile nature can easily break down into fine powders, which will hamper their practical applications.[37] To conquer this problem and investigate their potential applications in microplastics removal, methods that can fabricate MOFs into required shapes are necessary before they can be widely adopted in practical application scenarios.[38] We assume that the most suitable materials for efficient microplastic removal might have the following properties: (1) developed porosity to ensure high permeability of solvent for large-quantity filtration experiments; (2) proper force to guarantee the readily capture of microparticles and ease of recycling; (3) high durability that can tolerate harsh conditions; (4) ease of processing that can be fit to diverse devices. To this end, the best choice might be to select highly stable MOFs with rich functionality and fabricate them into powerful shapes like foams to meet the required demand. In the MOFs and foam material-integrated system, it can be assumed that foam-shaped materials with developed porosity might provide interpenetrated pore structures to ensure sufficient contact between microplastics and functional MOFs to achieve high removal efficiency.

As a proof-of-concept, melamine foam (MF),[39] a fluffy and porous foam with high flexibility, robustness and stability, was selected as the desired substrate to load stable zirconium MOFs (Zr-MOFs) and investigated their microplastic removal performances. We report herein, a unique acetone-assisted method for the preparation of various Zr-MOF-based foam materials and we successfully applied them in simulated microplastics removal (Fig. 1a). It can be extended to various functional Zr-MOF systems (UiO-66-X, X = H, NH_2, OH, Br and NO_2) with well-tuned MOF loadings. In particular, these foam materials possess high uniformity, robustness, flexibility and durability and are easy to scale-up. Moreover, these foam materials can be successfully applied in efficient simulated microplastics removal of various types or concentrations of microplastics suspensions. Notably, the best of them, UiO-66-OH@MF-3, shows high removal efficiency (up to 95.5 ± 1.2%) and can maintain high performance in recycling (10 cycles) or large-quantity filtration experiments. An automatic filtration system powered by sunlight was also proposed and accomplished on the lab-scale, which holds promise in the removal of microplastics in natural environments (Fig. 1b).

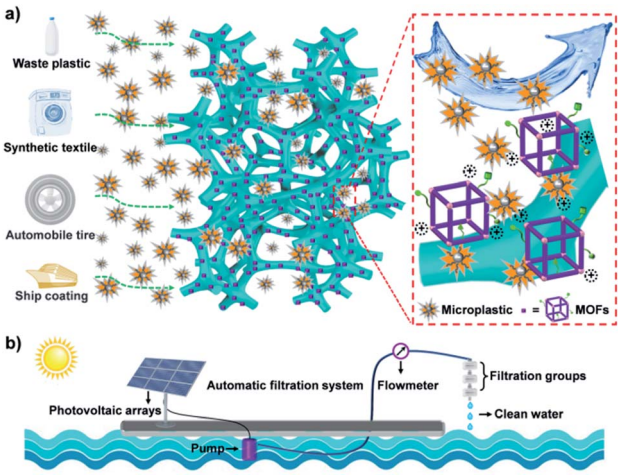

Fig. 1 (a) The schematic representation of MOF-based foam materials for microplastics removal. (b) The schematic representation of the automatic filtration system.

Results and discussion

The preparation of Zr-MOF-based foam materials through an acetone-assisted method is presented as follows. A certain amount of ligand and metal salt were mixed in acetone and stirred at room temperature to achieve a homogeneous solution. The solution was then added to an autoclave with a certain size of MF. After the solvothermal process, Zr-MOF was successfully synthesized and loaded onto the MF. Upon tuning the species and amounts of Zr-MOF precursors, this method could be extended into various MOF systems (UiO-66-X, X = H, NH_2, OH, Br and NO_2) with different loadings (UiO-66-X@MF-*n*, where *n* = 1–4 and represents the mass loading of MOFs ranging from 4.4 to 25.8 wt%).

Zr-based UiO-66-X (X = H, NH_2, OH, Br and NO_2) are stable MOFs constructed from the $Zr_6(OH)_4O_4$ cluster and the 1,4-dicarboxybenzene ligand with different functional groups (Fig. 2a and S1†).[40] Powder X-ray diffraction (PXRD) tests proved the successful formation of UiO-66-X (X = H, NH_2, OH, Br and NO_2) in the foam materials (Fig. S2†). Scanning electron microscopy (SEM) showed that all the MOF nanocrystals were uniformly distributed on the skeletons of MF with particle sizes between 100 and 200 nm (Fig. S1†). Taking UiO-66-OH@MF-3 for an example, the thickness (~1 cm) and shape of the foam material were almost unchanged as compared with the bare MF (Fig. S1c and S3†). In the SEM test, MF still possessed an interpenetrated pore structure and UiO-66-OH nanocrystals with ~152 nm in size were uniformly distributed on the surface of the MF skeletons as compared with that of bare MF (Fig. 2c, S1 and S3†). The uniformity of UiO-66-OH nanocrystals was further proved by the elemental mapping analysis (Fig. S4†).

Obtained from such a facile method, MOF loadings can be easily tuned through adjusting the amounts of metal salts and ligands. MOF loadings varying from 4.4 to 25.8 wt% were achieved for UiO-66-OH@MF-*n* (*e.g.*, UiO-66-OH@MF-1, 4.4 wt% and UiO-66-OH@MF-4, 25.8 wt%) (Table S1,† for details, see the

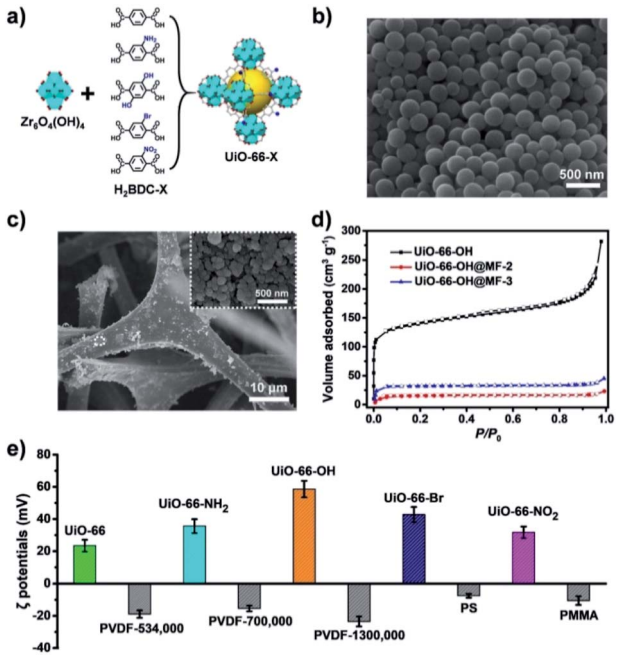

Fig. 2 (a) The structures of UiO-66-X (X = H, NH_2, OH, Br and NO_2). (b) The SEM image of PVDF nanoparticles (M_w 5.34 × 10^5 g mol^{-1}). (c) The SEM image of UiO-66-OH@MF-3 (inset is the zoomed-in image of the square area in c). (d) N_2 sorption curves of UiO-66-OH, UiO-66-OH@MF-2 and UiO-66-OH@MF-3. (e) The ζ potentials for various Zr-MOFs and microplastics.

Methods section). Furthermore, the PXRD patterns showed that UiO-66-OH@MF-*n* displayed a crystalline structure of UiO-66-OH (Fig. S5†). In particular, the MOF loading for UiO-66-OH@MF-4 (25.8 wt%) had a negligible change compared with that of UiO-66-OH@MF-3 (25.4 wt%), which implies that UiO-66-OH@MF-3 almost reached the saturation point of MOF loading. Besides, the distribution of UiO-66-OH nanocrystals on the surface of MF skeletons showed a trend from sparse to dense with the increase of the MOF loading (Fig. 2c and S6†). Overall, the UiO-66-OH-modified MF retained the interpenetrated pore structure, which is highly advantageous for further applications like microplastics removal.

Acetone is a polar solvent with small molecular size, which is generally applied as the replaced solvent to activate the pores of MOFs.[41] The facile method that directly utilizes acetone as a synthesis solvent can spontaneously activate the pores of the obtained samples. To prove this, N_2 sorption tests at 77 K were conducted for the as-prepared samples to investigate their porosity. The specific surface area (S_{BET}) and pore volume (V_t) of UiO-66-OH were calculated to be 527 m^2 g^{-1} and 0.34 cm^3 g^{-1}, respectively, which were consistent with the literature report (Fig. 2d and Table S1†).[42] Similar phenomena were also detected for the Zr-MOF-based foam materials. Taking UiO-66-OH@MF-2 and UiO-66-OH@MF-3 for instance, they exhibited the retained porosity of pristine UiO-66-OH (*i.e.* UiO-66-OH@MF-2, 62 m^2 g^{-1}, 0.022 cm^3 g^{-1} and UiO-66-OH@MF-3, 132 m^2 g^{-1}, 0.043 cm^3 g^{-1}) when their loadings were taken into consideration (Fig. 2d and Table S1†). The pore size distributions of UiO-66-OH@MF-2 and UiO-66-OH@MF-3 exhibited narrowly distributed micropores centered at ~0.80 nm, which matched well with that of UiO-66-OH (Fig. S7†).

Flexibility and robustness are important parameters to reflect the durability and persistence of the materials in real application scenarios.[38] MF, possessing various oxygen-based (*e.g.*, C=O, C–O, C–N and O–C=O) and nitrogen-based (*e.g.*, graphene-like, pyrrolic and pyridine-like nitrogen) functional groups as revealed by X-ray photoelectron spectroscopy (XPS), might provide a desirable platform for the loading of UiO-66-X (X = H, NH_2, OH, Br and NO_2) (Fig. S8†).[43] The obtained materials presented high robustness and their performances were tested by tensile stress tests. In particular, their performances (including strain (ε) and stress (δ)) decreased gradually with the increase in MOF loadings in the tests ((ε (%), δ (MPa)): MF (0.43, 0.071); UiO-66-OH@MF-1 (0.27, 0.11); UiO-66-OH@MF-2 (0.21, 0.090); UiO-66-OH@MF-3 (0.19, 0.070) and UiO-66-OH@MF-4 (0.17, 0.060)) (Fig. S9†). Interestingly, these Zr-MOF-based foam materials presented comparable or even higher performances than bare MF, suggesting that the introduction of MOF might strengthen the foam system. Despite high robustness, these materials also showed high flexibility and durability. Taking UiO-66-OH@MF-3 for an example, it has negligible weight loss after bending and twisting treatment (each for 100 times) (Fig. S10a†). Besides, it also maintained its weight and shape after a violent mechanical stirring test (200 rpm, 30 min), which simulated the condition that combines collision and pressing together (Fig. S10b†). It is noteworthy that UiO-66-X@MF exhibited high water stability when tested by immersing the sample in water for a certain time. The structural integrity of UiO-66-OH@MF-3 remained almost unchanged after immersion in water for more than a month, as compared with the as-synthesized structure (Fig. S11†). The high robustness, flexibility and durability of these Zr-MOF based foam materials set a fundamental basis for further applications.

As mentioned above, a series of Zr-MOF-based foam materials were obtained with uniformly distributed MOF nanocrystals, and accessible MOF porosity, which retained the strength and flexibility of the bare MF, showing great promise for microplastics removal. To assess the potential of these foam materials in microplastics removal, it was necessary to study the potential interaction between the foam materials and microplastics by determining the ζ potentials of various MOFs and microplastics. The ζ potentials of UiO-66, UiO-66-NH_2, UiO-66-OH, UiO-66-Br and UiO-66-NO_2 were determined to be 23.4 ± 3.7, 35.6 ± 2.3, 58.6 ± 5.1, 42.8 ± 4.7 and 31.7 ± 3.6 mV, respectively (Fig. 2e).[44,45] This result was also verified by the NH_3 temperature-programmed desorption tests (NH_3-TPD), in which UiO-66-OH exhibited the largest amount of defects and highest acid amount in UiO-66-X (Fig. S12†).[46–48] Therefore, UiO-66-OH was selected as the best example to investigate the possible influence effect on ζ potentials. To study this, different temperatures (*i.e.* 80, 90, 100 and 110 °C) were applied to successfully synthesize UiO-66-OH and their ζ potentials were tested (Fig. S13†). Interestingly, a volcano-shaped trend was observed (*i.e.* 80 °C, 48.3 ± 3.5 mV; 90 °C, 50.5 ± 4.0 mV; 100 °C 58.6 ± 5.1 mV and 110 °C, 53.1 ± 4.0 mV), which

could be ascribed to the diverse applied temperatures that would result in different amounts of exposed defects (Fig. S13b†). Moreover, most of the microplastics are negatively charged (*e.g.*, poly(vinylidene fluoride) (PVDF), −18.9 ± 2.3 mV; polystyrene (PS), −7.5 ± 1.2 mV and polymethylmethacrylate (PMMA), −10.5 ± 2.7 mV; *etc.*) (Fig. 2e). Besides, microplastics like PVDF have numerous –CF_2– units, which might generate hydrogen bonding in water with the functional groups in MOFs and PVDF (*e.g.*, the hydrogen bond energy for OH···F is 2.4 kJ mol^{-1}).[49] As mentioned above, the potential applications of these Zr-MOF based foam materials in microplastic removal might be as follows: (1) the uniformly distributed MOF nanoparticles with abundant positive charges might have strong electrostatic interactions with negatively charged microplastics. (2) MOF nanoparticles with numerous functional groups or defects might possess potential interactions like hydrogen bonds or van der Waals interactions with microplastics. (3) The developed and interpenetrated pore structure of MF can ensure the rapid passage of solvent, with sufficient contact between the microplastics and MOF nanoparticles. (4) The good water stability of Zr-MOFs combined with the high strength and flexibility of MF might endow these foam materials with many advantages in the fabrication, transportation or large-quantity filtration applications.

As a proof-of-concept, we set out to investigate the simulated microplastics removal performances of the Zr-MOF-based foam materials. A typical filtration device was applied to filter the microplastics (Fig. S14,† for details, see the Methods section). Various UiO-66-X@MF were used as the filters and the PVDF (M_w 5.34 × 10^5 g mol^{-1}) nanoparticle suspension was selected as the simulated microplastic suspension (Fig. 2b). PVDF nanoparticles purchased from commercial sources presented an average diameter of ∼260 nm in the SEM tests (Fig. 2b). As verified by the dynamic light scattering (DLS) tests, the PVDF nanoparticles were uniformly dispersed in the simulated microplastics suspension with a measured size of ∼273 nm, which was consistent with the results from SEM tests (Fig. S15†). UiO-66-X@MF exhibited high removal efficiency (*i.e.* UiO-66@MF, 65.6 ± 3.7%; UiO-66-NH_2@MF, 75.3 ± 2.8%; UiO-66-OH@MF, 90.1 ± 2.1%; UiO-66-Br@MF, 61.8 ± 3.2% and UiO-66-NO_2@MF, 62.0 ± 4.2%) as compared with bare MF (33.0 ± 2.6%) (Fig. 3a). UiO-66-OH@MF exhibited the highest performance as compared with other foam materials, which matched well with the ζ potentials and NH_3-TPD tests as mentioned above. Therefore, UiO-66-OH@MF with the best removal performance was selected as the desired example to further investigate the possible influencing factors relevant to the removal efficiency. For UiO-66-OH@MF with different UiO-66-OH loadings, the removal efficiency increased with the enhancement of the UiO-66-OH loading (*i.e.* UiO-66-OH@MF-1, 51.7 ± 3.3%; UiO-66-OH@MF-2, 77.8 ± 4.2% and UiO-66-OH@MF-3, 90.1 ± 2.1%) (Fig. 3b). UiO-66-OH@MF-3 prepared at different temperatures, as verified by PXRD and SEM tests, were also studied in simulated microplastics removal (Fig. S16 and S17†). In particular, UiO-66-OH@MF-3 prepared at different temperatures showed slightly different removal efficiencies (80 °C, 85.3 ± 3.7%; 90 °C, 88.2 ± 2.8%; 100 °C, 90.1 ± 2.1% and 110 °C, 87.2 ± 3.2%), in good agreement with the ζ potential result (Fig. S13b and S18†).

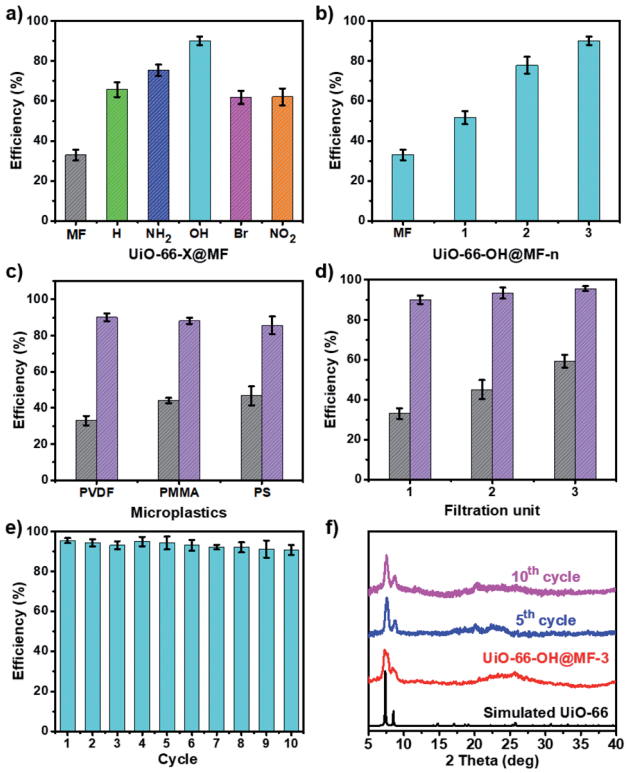

Fig. 3 (a) The removal efficiency of UiO-66-X@MF (X = X = H, NH_2, OH, Br and NO_2). (b) The removal efficiency of UiO-66-OH@MF-*n* (*n* = 1–3). (c) The removal efficiency of UiO-66-OH@MF-3 for different microplastics types. (d) The removal efficiency of UiO-66-OH@MF-3 with different filtration units. (e) The recycling performances of UiO-66-OH@MF-3-based filtration groups (three units). (f) The PXRD patterns of UiO-66-OH@MF-3 after the recycling tests.

The above results inspired us to explore the versatility of these Zr-MOF based foam materials in microplastics removal. The simulated microplastics suspension with different types of microplastics (including diverse species and particle sizes) and various concentrations were investigated. UiO-66-OH@MF-3 presented higher removal performances in the removal of various types of microplastics (*i.e.* PMMA, 88.2 ± 1.7% and PS, 85.7 ± 4.8%) as compared with that of bare MF (*i.e.* PMMA, 44.1 ± 1.4% and PS, 46.7 ± 5.2%) (Fig. 3c). The diverse removal performances might be ascribed to factors like the particle size (*e.g.*, PVDF, ∼260 nm; PMMA, ∼325 nm and PS, ∼183 nm) or ζ potentials (*e.g.*, PVDF, −18.9 ± 2.3 mV; PS, −7.5 ± 1.2 mV and PMMA, −10.5 ± 2.7 mV) of different microplastics (Fig. 2e and S19†). To further study the effects of the microplastics particle size on the removal efficiency, PVDF with different M_w, possessing various particle sizes (*i.e.* 5.34 × 10^5 g mol^{-1}, ∼260 nm; 7.0 × 10^5 g mol^{-1}, ∼300 nm and 1.3 × 10^6 g mol^{-1}, ∼322 nm), were selected as the desired examples. UiO-66-OH@MF-3 showed almost the same removal efficiency for microplastics with different particle sizes (∼260 nm, 90.1 ± 2.1%; ∼300 nm, 90.6 ± 1.8% and ∼322 nm, 89.8 ± 1.2%), which implies that the ζ potentials might play a more important role in microplastics

removal than particle size (Fig. S19 and S20a†). In real scenarios, the concentrations of microplastics differ a lot and it is necessary to investigate microplastics suspensions with various concentrations. The concentration of PVDF (M_w 5.34 × 10^5 g mol^{-1}) based microplastic suspension was tuned from 0.5 to 2.0 g L^{-1}, which was much higher than that in the natural environment, and this served as the simulated microplastics suspension under lab conditions.[11] After filtration, UiO-66-OH@MF-3 showed high removal efficiency for all concentrations (*i.e.* 0.5 g L^{-1}, 89.6 ± 2.8%; 1.0 g L^{-1}, 90.1 ± 2.1% and 2.0 g L^{-1}, 88.2 ± 3.2%), implying the applicability of this material in complex natural conditions with diverse microplastics concentrations (Fig. S20b†). To further increase the removal efficiency, multiple filtration units can be readily connected in series to achieve higher performance. For example, the removal efficiency of UiO-66-OH@MF-3 was enhanced accordingly with the increased number of filtration units (one unit, 90.1 ± 2.1%; two units, 93.4 ± 2.7% and three units, 95.5 ± 1.2%) (Fig. 3d).

The superiority of these Zr-MOF-based foam materials in microplastics removal was further supported by the contrast experiments of other filtration materials (*e.g.*, filter paper (20–25 μm) and microfiltration membrane (~0.22 μm)) conducted under similar conditions (Fig. S21†).[17] The filter paper showed a lower removal efficiency of 65.2 ± 5.2% than that of UiO-66-OH@MF-3 (90.1 ± 2.1%) under similar conditions (Fig. S21c†). The lower efficiency might be ascribed to the relatively large pore size of the filter paper (20–25 μm) so micron- or nanometer-sized microplastics were difficult to remove efficiently (Fig. S21a and c†). The flow rate of the solvent for filter paper (~0.15 L h^{-1}) was also slower as compared with that of UiO-66-OH@MF (~1.2 L h^{-1}) under normal pressure. For the microfiltration membrane, it could not even achieve the successful filtration of microplastics under normal pressure. This might be attributed to the small pore sizes (~0.22 μm) of the microfiltration membrane, which would be easily blocked by microplastics to terminate the filtration process (Fig. S21b and c†). These results further revealed the advantages of the Zr-MOF-based foam materials with developed and interpenetrated pore structures in microplastics removal.

Recyclability is an important parameter for studying the durability of these Zr-MOF-based foam materials.[50] The UiO-66-OH@MF-3 based filtration group (three units) with the best performance (95.5 ± 1.2%) was selected as the desirable platform for investigating the recycling performance. It is noteworthy that it can be reused in the repetitive removal of microplastics with high removal efficiency (removal efficiency, 95.5 ± 1.2% (first run), 93.1 ± 2.1% (third run), 94.3 ± 3.2% (fifth run), 92.2 ± 1.2% (seventh run), and 90.7 ± 2.3% (tenth run)) (Fig. 3e). The structural integrity of UiO-66-OH@MF-3 remained intact after the recycling experiments (Fig. 3f). SEM analysis of UiO-66-OH@MF-3 after microplastics removal tests indicated that PVDF-based microplastics with a size of ~263 nm can be readily observed on the skeleton surface of UiO-66-OH@MF-3, which implies the possible interaction between UiO-66-OH and microplastics (Fig. S1, S19 and S22†). Moreover, UiO-66-OH@MF-3 after filtration exhibited a C–F stretching peak at 1186.5 cm^{-1} in the Fourier Transform Infrared (FT-IR) spectrum when compared with that of PVDF and UiO-66-OH@MF-3, which further supports the existence of PVDF microplastics (Fig. S23†). The filtered PVDF-based microplastics in UiO-66-OH@MF-3 can be removed by washing with water several times as proved by the SEM tests (Fig. S22c and d†). The N_2 sorption test was further carried out to evaluate the porosity of UiO-66-OH@MF-3 after filtration. The S_{BET} (121 m^2 g^{-1}) and V_t (0.31 cm^3 g^{-1}) were slightly decreased with similar pore size distribution as compared with that of UiO-66-OH@MF-3 before filtration (S_{BET}, 132 m^2 g^{-1} and V_t, 0.34 cm^3 g^{-1}), implying the high durability of the foam material (Fig. S24†). Moreover, the production of these Zr-MOF-based foam materials with high recyclability could be easily scaled-up. When the reaction conditions were expanded to five times, the foam material (5 × 5 cm^2) with a larger size was successfully obtained as proved by the PXRD test (Fig. S25a and b†). The foam material obtained from the scale-up conditions could still maintain the high removal efficiency, which holds high promise in practical applications (Fig. S25b†).

The study of large-quantity filtration tests is essential for practical applications. For the large-quantity filtration test, 1 L of the PVDF-based microplastics suspension was filtered through UiO-66-OH@MF-3-based filtration groups (three units) under normal pressure (Fig. 4a). After the large-quantity filtration experiment (~4 h), 85.2 ± 5.3% removal efficiency was achieved for the UiO-66-OH@MF-3-based filtration groups (three units) (Fig. S26†). The large-quantity filtration could also be recycled for three cycles with slightly decreased removal efficiency (removal efficiency: 85.2 ± 5.3% (first run), 83.7 ± 4.8% (second run) and 83.9 ± 6.4% (third run)) (Fig. S26†).

In real scenarios, most microplastics are distributed in seawater and lots of materials like ions or organic matter can be adsorbed on the surface of the microplastics. Therefore, the investigation of the filtration performance under various conditions is necessary. The stability tests of UiO-66-OH or UiO-66-OH@MF-3 were first conducted and they both exhibited retained crystallinity like that of the pristine sample in organic

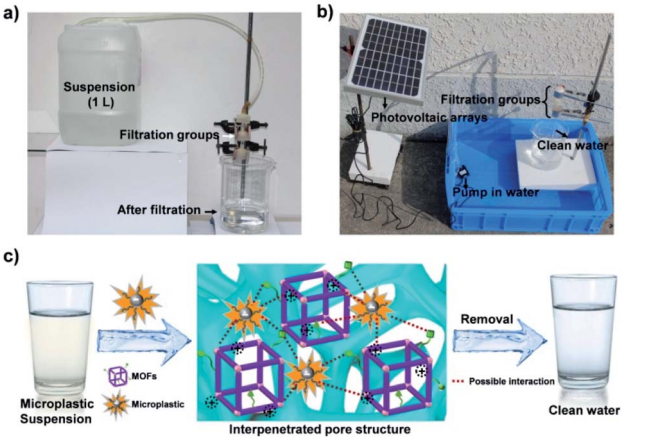

Fig. 4 (a) Photographs of the device for large-quantity filtration testing (flow rate: ~0.25 L h^{-1}). (b) The photo of the automatic filtration system on the lab-scale. (c) Schematic representation of the possible interactions between microplastics and foam materials.

solvents, acid/base or seawater conditions (Fig. S27a and S28†). In simulated seawater conditions, the UiO-66-OH@MF-3-based filtration groups (three units) presented a slightly decreased removal efficiency (94.2 ± 3.2%) for the removal of PVDF-based microplastics when compared with that in water (95.5 ± 1.2%) (Fig. S27b†). We also conducted experiments to explore the performances of the foam materials for microplastics systems with the addition of organic molecules (*e.g.*, polyethylene glycol (PEG, 4.0×10^3 g mol^{-1}) and polyvinylpyrrolidone (PVP, 5.2×10^4 g mol^{-1})). We found that the performances of the foam materials could be maintained after the filtration of microplastics suspensions with the addition of different organic molecules (*i.e.* PEG, 89.2 ± 1.4%; PVP, 90.3% ± 1.8%) when compared with suspensions without organic molecules (90.1 ± 2.1%) (Fig. S29†).

Based on the high filtration efficiency mentioned above, an automatic filtration system powered by the sunlight was proposed. As shown in the schematic presentation image in Fig. 1b, a platform system, including photovoltaic arrays, pump and filtration groups, was floating in the sea. On sunny days, the photovoltaic arrays will receive sunlight and transform it into electric energy to power the pump in the sea. The pump can draw the microplastics-contaminated seawater to pass through the filtration groups. After filtration, the clean seawater will go back into the sea. As a proof-of-concept, a simulated automatic filtration system was designed on the lab-scale and the system was successfully powered by the sunlight to pump water through the filtration groups (three units) (Fig. 4b). With the progressive development of photovoltaic materials like polysilicon and perovskites, higher sunlight-to-electricity efficiency will be achieved in the future. We can envision that the automatic filtration system might be a promising alternative for removing microplastics in real scenarios.

Based on the above-mentioned results, the advantages of the Zr-MOF-based foam materials in microplastics removal are as follows (Fig. 4c and S30†). Firstly, MF, with the interpenetrated pore structure and numerous functional sites can provide the desired platform to anchor Zr-MOFs, ensuring the fast passage of solvent and adequate contact of the microplastics with the skeleton (Fig. 4c and S30†). Secondly, UiO-66-X (X = H, NH_2, OH, Br and NO_2) with high stability are uniformly distributed on the skeletons of MF, thus showing high contact potential for the interaction between microplastics and MOFs. Thirdly, the nano-sized UiO-66-X (X = H, NH_2, OH, Br and NO_2) possessing numerous defects are positively charged, which would show a high affinity for negatively charged microplastics (*e.g.*, PVDF, PS and PMMA, *etc.*). Fourthly, the functional groups in Zr-MOFs provide further interactions like hydrogen bonding or van der Waals interactions with the microplastics. Therefore, the possible factors like the interpenetrated pore structure of MF, the positive charges or functional groups of Zr-MOFs, and the negative charge of microplastics were intensively investigated and discussed, and could contribute to the high performances of these Zr-MOF-based foam materials (Fig. 4c and S30†). However, the microplastics in water are a complicated system, so the Zr-MOF-based foam materials[51] require tremendous efforts to take all of the potential factors into consideration to reveal the possible mechanism during the microplastics removal processes.

Conclusions

In summary, a series of Zr-MOFs-based foam materials have been facilely fabricated through a unique acetone-assisted method. This method can be extended to various functional Zr-MOF systems (UiO-66-X, X = H, NH_2, OH, Br and NO_2) with well-tuned MOF loadings. The integration of stable Zr-MOFs with MF to give Zr-MOF-based foam materials possessing high uniformity, robustness and durability can be applied in efficient microplastics removal that is suitable for various types or concentrations of simulated microplastics suspensions. It is worth noting that the best of them, UiO-66-OH@MF-3, can efficiently remove microplastics with an efficiency of up to 95.5 ± 1.2% and can maintain high efficiency in recycling (10 cycles) and large-quantity filtration experiments. The characteristics of the obtained Zr-MOF-based foam materials and microplastics, such as the interpenetrated pore structure, ζ potential, or functional groups, have been intensively investigated and discussed to reveal the high efficiency of these Zr-MOF-based foam materials in microplastics removal. We further briefly investigated the filtration performance of these materials in simulated seawater conditions and proposed an automatic filtration system powered by sunlight. These powerful Zr-MOF-based foam materials possessing high efficiency in microplastic removal might provide a promising alternative to address the microplastic problems that are getting worse year after year.

Methods

Materials

All solvents and reagents obtained from commercial sources were used without further purification. $ZrCl_4$ (98%) was obtained from Acros Chemicals. Terephthalic acid (H_2BDC, 99%), 2-aminoterephthalic acid (H_2BDC-NH_2, 98%), 2,5-dihydroxyterephthalic acid (H_2BDC-OH 98%), 2-bromoterephthalic acid (H_2BDC-Br, 98%) and nitroterephthalic acid (H_2BDC-NO_2, 98%) were purchased from Aladdin Reagents. Poly(vinylidene fluoride) (PVDF, 5.34×10^5 g mol^{-1}) and poly(methyl methacrylate) (PMMA, 4.43×10^5 g mol^{-1}) were obtained from Alfa Aesar. Acetone, ethanol and *N*,*N*-dimethylformamide (DMF) were purchased from Sinopharm Chemical Reagent Co., Ltd., with purity >99%. PVDF (7.0×10^5 and 1.3×10^6 g mol^{-1}), melamine foam (MF), poly(-styrene) (PS, 1.92×10^5 g mol^{-1}) and seawater (Yellow Sea, Qingdao, China) were obtained from commercial sources.

Characterization and instruments

Powder X-ray diffraction (PXRD) patterns of samples were obtained using a D/max 2500 VL/PC diffractometer (Japan) equipped with Cu Kα radiation ($\lambda = 1.54060$ Å). Field-emission scanning electron microscopy (FESEM, S-4800) was applied to investigate the morphology of the samples. N_2 sorption tests were measured using a Bruker D8 Advance automatic volumetric gas sorption analyzer and the samples were pretreated at

150 °C for 24 h. X-ray photoelectron spectroscopy (XPS) measurements were performed on an American Thermo-VG Scientific ESCALAB 250XI XPS system with Al Kα radiation as the exciting source. The ζ potentials were measured by a JS94H micro-electrophoresis apparatus. The dynamic light scattering (DLS) was conducted *via* a Nanotrac Wave II (Microtrack, Boston, MA, USA); the instrument measures particles ranging in size from 0.8 to 6500 nm. The NH_3 temperature program desorption tests (NH_3-TPD) were conducted *via* the pulse technique using a Micromeritics AutoChem II 2920 instrument with TCD detection. The Fourier Transform Infrared (FT-IR) spectra were recorded from KBr pellets in the range of 400–4000 cm^{-1} on a Nicolet 170 SXFT-IR spectrometer.

Syntheses of UiO-66-X@MF (X = H, NH_2, OH, Br and NO_2)

A mixture of $ZrCl_4$ (90 mg, 0.39 mmol) and 2,5-dihydroxyterephthalic acid (77 mg, 0.39 mmol) was added to 30 mL acetone with stirring, followed by ultrasound for 30 min. The mixed solution and a piece of MF (thickness, ~1 cm) were sealed in a 50 mL Teflon-lined stainless-steel autoclave and heated at 100 °C for 24 h. After cooling to room temperature, the obtained foam material was washed 3 times with acetone and ethanol under stirring (each time for 3 h). After drying at 150 °C for 12 h under vacuum, UiO-66-OH@MF was obtained for further characterization. The UiO-66-OH loading in UiO-66-OH@MF was detected to be ~25.4 wt%.

For the syntheses of UiO-66-X@MF (X = H, NH_2, Br and NO_2), the procedures were similar to that of UiO-66-OH@MF, except that 2,5-dihydroxyterephthalic acid (77 mg, 0.39 mmol) was replaced by terephthalic acid (63 mg, 0.39 mmol), 2-aminoterephthalic acid (72 mg, 0.39 mmol), 2-bromoterephthalic acid (95 mg, 0.39 mmol) or nitroterephthalic acid (86 mg, 0.39 mmol).

For the syntheses of UiO-66-OH@MF-*n* with different loadings, the obtained UiO-66-OH@MF with ~25.4 wt% loading was defined as UiO-66-OH@MF-3. For other UiO-66-OH@MF-*n* ($n = 1$, 2 and 4), various amounts of precursors following the corresponding mole ratios (the ratio of *n*) in comparison to UiO-66-OH@MF-3 were added. Following the similar procedures, UiO-66-OH@MF-*n* was obtained and the results of MOF loadings were calculated (Table S1†).

The loadings of UiO-66-OH@MF-*n* ($n = 1$, 2, 3 and 4) were calculated through a simple weighing method. The masses of the foam materials before and after reaction were determined and recorded as m_1 (bare MF) and m_2 (UiO-66-X@MF), respectively. The loading of UiO-66-OH@MF-*n* was calculated as follows: loading (wt%) = $(m_2 - m_1)/m_1$. All the loading data were calculated at least three times to give the average.

Microplastics removal tests of UiO-66-X@MF (X = H, NH_2, OH, Br and NO_2)

For the preparation of a simulated microplastics suspension with a concentration of ~0.001 g mL^{-1}, ~0.2 g microplastic powder was added to a 200 mL mixture solution of H_2O and ethanol (volume ratio, 3 : 1) and ultrasonicated for 1 h to achieve a homogeneously dispersed suspension. Because most of the microplastics (*e.g.*, PVDF, PS and PMMA, *etc.*) easily agglomerate in water, it is necessary to add a small amount of ethanol to ensure the uniform dispersion. Taking PVDF (M_w 5.34 × 10^5 g mol^{-1}) as an example, the PVDF nanoparticles can be uniformly dispersed in the simulated microplastic suspension with a measured size of ~273 nm in the dynamic light scattering (DLS) tests, which is consistent with the results from SEM tests (~260 nm) (Fig. 2b and S15a†). In contrast, it is hard to uniformly disperse PVDF nanoparticles in water, as proved by the large particle size (1352 nm) detected in the DLS test (Fig. S15b†).

After the preparation of the simulated microplastics suspension, the foam materials (thickness, ~1 cm) were filled in the filter and pre-wetted (Fig. S14†). A certain amount of simulated microplastic suspension was filtered through the filter with a flow rate of ~1.2 L h^{-1} (Fig. S14†). After filtration, the filtered solution was collected. For the test of removal efficiency, two clean beakers (numbered A and B, 50 mL) with detected quality (m_{A1}, m_{B1}) were filled with 20 mL of simulated microplastic suspension and filtered solution, respectively. The beakers with solutions were transferred to an oven and dried at 140 °C for 6 h. During the heating process, the beakers were covered with watch glasses to avoid pollution. After cooling to room temperature, the weights of the beakers were calculated to be m_{A2} and m_{B2}. The concentration of the simulated microplastic suspension (C_1) was calculated $C_1 = (m_{A2} - m_{A1})/V$. Similarly, the concentration of the filtered solution (C_2) was calculated as $C_2 = (m_{B2} - m_{B1})/V$. The filtration efficiency (FE) was calculated as FE = $[(C_1 - C_2)/C_1] \times 100\%$. For the microplastics removal experiment in simulated seawater (obtained from a commercial source, Yellow Sea, Qingdao, China), the procedures were the same as that in water. In the tests, more than three groups of concentration data were collected in a single experiment to give the average result. All the filtration tests were conducted in triplicate.

The large-quantity filtration and recycle experiments

For the large-quantity filtration, 1 L PVDF (M_w 5.34 × 10^5 g mol^{-1}) based simulated microplastics suspension (~0.001 g mL^{-1}) was filtered through three connected filtration units (UiO-66-OH@MF-3 inside) (Fig. 4a). After ~4 h, the filtered solution was collected to detect the concentration and calculate the filtration efficiency. For the recycling experiments, UiO-66-OH@MF-3-based three connected filtration units were applied to repetitively filter 20 mL PVDF (M_w 5.34 × 10^5 g mol^{-1}) based simulated microplastics suspension (~0.001 g mL^{-1}) for 10 cycles. After filtration, UiO-66-OH@MF-3 was washed 3 times with water under stirring (every time for 3 h) and dried at 150 °C for 12 h under vacuum. After drying, the recycled sample was directly used in the next cycling experiment. For large-quantity filtration and recycling experiments, all the filtration tests were conducted in triplicate to give the average data.

Author contributions

Y.-J. C., Y. C., and Y.-Q. L. conceived the idea. Y.-J. C., Y. C., S.-L. L. and Y.-Q. L. designed the experiments, collected and analyzed the data. Y.-J. C., Y.-R. W., G.-K. G., H.-J. Z., R.-X. Y., C. M. and J.-H. W. assisted with the experiments and

characterizations. Y.-J. C. and Y. C. wrote the manuscript. All authors discussed the results and commented on the manuscript.

Conflicts of interest

There are no conflicts to declare.

Acknowledgements

This work was financially supported by NSFC (No. 21701085, 21871141, 21871142 and 21901122); the NSF of Jiangsu Province of China (No. BK20171032); the Natural Science Research of Jiangsu Higher Education Institutions of China (No. 17KJB150025 and 19KJB150011) and Project funded by China Postdoctoral Science Foundation (No. 2018M630572 and 2019M651873); Priority Academic Program Development of Jiangsu Higher Education Institutions and the Foundation of Jiangsu Collaborative Innovation Center of Biomedical Functional Materials.

References

1 M. A. Hillmyer, *Science*, 2017, **358**, 868.
2 R. Geyer, J. R. Jambeck and K. L. Law, *Sci. Adv.*, 2017, **3**, e1700782.
3 H. Sardon and A. P. Dove, *Science*, 2018, **360**, 380–381.
4 A. A. Shah, F. Hasan, A. Hameed and S. Ahmed, *Biotechnol. Adv.*, 2008, **26**, 246–265.
5 L. Lebreton, M. Egger and B. Slat, *Sci. Rep.*, 2019, **9**, 12922.
6 R. C. Thompson, *Science*, 2004, **304**, 838.
7 A. L. Lusher, V. Tirelli, I. O'Connor and R. Officer, *Sci. Rep.*, 2015, **5**, 14947.
8 J. R. Jambeck, R. Geyer, C. Wilcox, T. R. Siegler, M. Perryman, A. Andrady, R. Narayan and K. L. Law, *Science*, 2015, **347**, 768–771.
9 M. Yurtsever, *J. Agric. Environ. Ethics*, 2019, **32**, 459–478.
10 R. Dris, J. Gasperi, M. Saad, C. Mirande and B. Tassin, *Mar. Pollut. Bull.*, 2016, **104**, 290–293.
11 D. Cressey, *Nature*, 2016, **536**, 263–265.
12 T. S. Galloway and C. N. Lewis, *Proc. Natl. Acad. Sci. U. S. A.*, 2016, **113**, 2331–2333.
13 S. Sharma and S. Chatterjee, *Environ. Sci. Pollut. Res. Int.*, 2017, **24**, 21530–21547.
14 Y. Ku, P. Lee and W. Wang, *J. Membr. Sci.*, 2005, **250**, 159–165.
15 J. J. Porter and A. C. Gomes, *Desalination*, 2000, **128**, 81–90.
16 J. Wang, J. X. Wong, H. Kwok, X. Li and H. Z. Yu, *PLoS One*, 2016, **11**, e0151439.
17 M. Lares, M. C. Ncibi and M. Sillanpää, *Water Res.*, 2018, **133**, 236–246.
18 F. Lagarde, O. Olivier, M. Zanella, P. Daniel, S. Hiard and A. Caruso, *Environ. Pollut.*, 2016, **215**, 331–339.
19 W. Perren, A. Wojtasik and Q. Cai, *ACS Omega*, 2018, **3**, 3357–3364.
20 K. Gurung, M. C. Ncibi, J. M. Fontmorin, H. Särkkä and M. Sillanpää, *J. Membr. Sci. Technol.*, 2016, **6**, 100158.
21 M. Padervand, E. Lichtfouse, D. Robert and C. Wang, *Environ. Chem. Lett.*, 2020, **18**, 807–828.
22 S. Yuan, L. Feng, K. Wang, J. Pang, M. Bosch, C. Lollar, Y. Sun, J. Qin, X. Yang, P. Zhang, Q. Wang, L. Zou, Y. Zhang, L. Zhang, Y. Fang, J. Li and H. C. Zhou, *Adv. Mater.*, 2018, **30**, e1704303.
23 H. Furukawa, U. Muller and O. M. Yaghi, *Angew. Chem., Int. Ed.*, 2015, **54**, 3417–3430.
24 R. Kitaura, *Science*, 2002, **298**, 2358–2361.
25 H. Li, M. Eddaoudi, M. O'Keeffe and O. M. Yaghi, *Nature*, 1999, **402**, 276–279.
26 R. W. Huang, Y. S. Wei, X. Y. Dong, X. H. Wu, C. X. Du, S. Q. Zang and T. C. W. Mak, *Nat. Chem.*, 2017, **9**, 689–697.
27 P. Z. Li, X. J. Wang, J. Liu, J. S. Lim, R. Zou and Y. Zhao, *J. Am. Chem. Soc.*, 2016, **138**, 2142–2145.
28 B. Aguila, Q. Sun, X. Wang, E. O'Rourke, A. M. Al-Enizi, A. Nafady and S. Ma, *Angew. Chem., Int. Ed.*, 2018, **57**, 10107–10111.
29 S. M. Towsif Abtab, D. Alezi, P. M. Bhatt, A. Shkurenko, Y. Belmabkhout, H. Aggarwal, Ł. J. Weseliński, N. Alsadun, U. Samin, M. N. Hedhili and M. Eddaoudi, *Chem*, 2018, **4**, 94–105.
30 R. B. Lin, S. Xiang, H. Xing, W. Zhou and B. Chen, *Coord. Chem. Rev.*, 2019, **378**, 87–103.
31 T. Islamoglu, S. Goswami, Z. Li, A. J. Howarth, O. K. Farha and J. T. Hupp, *Acc. Chem. Res.*, 2017, **50**, 805–813.
32 A. Dhakshinamoorthy, Z. Li and H. Garcia, *Chem. Soc. Rev.*, 2018, **47**, 8134–8172.
33 H. Furukawa, K. E. Cordova, M. O'Keeffe and O. M. Yaghi, *Science*, 2013, **341**, 1230444.
34 Y. Zhang, S. Yuan, X. Feng, H. Li, J. Zhou and B. Wang, *J. Am. Chem. Soc.*, 2016, **138**, 5785–5788.
35 P. A. Kobielska, A. J. Howarth, O. K. Farha and S. Nayak, *Coord. Chem. Rev.*, 2018, **358**, 92–107.
36 M. Mon, R. Bruno, J. Ferrando-Soria, D. Armentano and E. Pardo, *J. Mater. Chem. A*, 2018, **6**, 4912–4947.
37 A. U. Czaja, N. Trukhan and U. Muller, *Chem. Soc. Rev.*, 2009, **38**, 1284–1293.
38 Y. Chen, S. Zhang, S. Cao, S. Li, F. Chen, S. Yuan, C. Xu, J. Zhou, X. Feng, X. Ma and B. Wang, *Adv. Mater.*, 2017, **29**, 1606221.
39 A. Stolz, S. Le Floch, L. Reinert, S. M. M. Ramos, J. Tuaillon-Combes, Y. Soneda, P. Chaudet, D. Baillis, N. Blanchard, L. Duclaux and A. San-Miguel, *Carbon*, 2016, **107**, 198–208.
40 L. Valenzano, B. Civalleri, S. Chavan, S. Bordiga, M. H. Nilsen, S. Jakobsen, K. P. Lillerud and C. Lamberti, *Chem. Mater.*, 2011, **23**, 1700–1718.
41 L. A. Lozano, C. M. Iglesias, B. M. C. Faroldi, M. A. Ulla and J. M. Zamaro, *J. Mater. Sci.*, 2018, **53**, 1862–1873.
42 J. Li, Q. Wu, X. Wang, Z. Chai, W. Shi, J. Hou, T. Hayat, A. Alsaedi and X. Wang, *J. Mater. Chem. A*, 2017, **5**, 20398–20406.
43 N. Huang, H. Drake, J. Li, J. Pang, Y. Wang, S. Yuan, Q. Wang, P. Cai, J. Qin and H. C. Zhou, *Angew. Chem., Int. Ed.*, 2018, **57**, 8916–8920.
44 M. A. Nasalevich, M. van der Veen, F. Kapteijn and J. Gascon, *CrystEngComm*, 2014, **16**, 4919–4926.

45 S. Li, S. Sun, H. Wu, C. Wei and H. Yun, *Catal. Sci. Technol.*, 2018, **8**, 1696–1703.
46 Y. Pan, B. Yuan, Y. Li and D. He, *Chem. Commun.*, 2010, **46**, 2280–2282.
47 H. Jiang, Q. Wang, H. Wang, Y. Chen and M. Zhang, *ACS Appl. Mater. Interfaces*, 2016, **8**, 26817–26826.
48 J. Jiang and O. M. Yaghi, *Chem. Rev.*, 2015, **115**, 6966–6997.
49 M. A. Biamonte and A. Vasella, *Helv. Chim. Acta*, 1998, **81**, 695–717.
50 G. Ji, Z. Yang, H. Zhang, Y. Zhao, B. Yu, Z. Ma and Z. Liu, *Angew. Chem., Int. Ed.*, 2016, **55**, 9685–9689.
51 M. Enfrin, L. F. Dumee and J. G. Lee, *Water Res.*, 2019, **161**, 621–638.